Smart Structures and Systems, *Vol. 35*, *No. 1* (*2025*) *53-64*
https://doi.org/10.12989/sss.2025.35.1.053

Detection of wire breakage in steel strands using a roving magnetostrictive guided wave detector and outlier analysis

Xiaodong Sui [1,2,3a], Ru Zhang*[2,3], Yuanfeng Duan [1b], Yaozhi Luo [1c] and Chungbang Yun [1d]

[1] *College of Civil Engineering and Architecture*, *Zhejiang University*, *China*
[2] *Department of Civil Engineering*, *Hangzhou City University*, *China*
[3] *Key Laboratory of Safe Construction and Intelligent Maintenance for Urban Shield Tunnels of Zhejiang Province*, *Hangzhou City University*, *China*

(*Received October 25*, *2024*, *Revised January 8*, *2025*, *Accepted January 21*, *2025*)

Abstract. It is crucial to detect the local damages on steel strands and cables to ensure the safety of a cable-supported structure. A magnetostrictive (MS) guided wave-based method for local wire breakage condition assessment is presented in this study. Traditional guided wave-based structure health monitoring methods, which rely on damage-reflected wave packets, often struggle with the challenge of significant wave energy attenuation over long propagation distances. To overcome this problem, a damage detector comprising a pair of MS transducers was developed. The detector is designed to move along the steel strand, obtaining the transmitted wave energy at various locations. An outlier analysis was conducted by taking the transmitted wave energy as a feature sensitive to damage. The threshold value for the transmitted wave energy was determined for wire breakage detection and localization, and the wave energy transmission coefficient was employed for local damage severity estimation. Numerical and experimental studies were carried out on a seven-wire steel strand with a single wire breakage case. The results demonstrate that the damage location and local damage severity can be estimated accurately using the proposed method.

Keywords: outlier analysis; roving magnetostrictive guided wave detector; steel strand; wave energy method; wire breakage

1. Introduction

Steel strands are extensively used on various structures across a diverse range of industries, including cable-supported bridges, power transmission lines, and elevators, where they play a crucial role in the whole structure (Rizzo and di Scalea 2006, Abdullah *et al*. 2015, Rostami *et al*. 2020). However, local damages, such as wire breakage and corrosion, may occur within the steel strands during the service life due to the harsh operating and environmental conditions, resulting in the reduction of the load carrying capacities. Therefore, it is imperative to monitor the local damages in the steel strand to prevent catastrophic accidents (Kharrat and Gaillet 2015, Dubuc *et al*. 2018). Recently, many nondestructive testing methods have been presented to assess the local damage conditions of the steel strands, including the electromechanical impedance method, acoustic emission method, magnetic flux leakage method, and ultrasonic guided wave method (Christen *et al*. 2009, Nguyen and Kim 2012, Ibáñez *et al*. 2015, Wu *et al*. 2018). However, some of these methods face challenges in real engineering applications owing to the limitations in terms of sensing range and accuracy. Researches on the ultrasonic guided wave method have shown that it can achieve high accuracy and efficiency in damage detection. Various guided wave methods have been successfully applied in pipes, beams, bolt connected joints, cables, and rails (Setshedi *et al*. 2019, Duan *et al*. 2022, Ng *et al*. 2022, Tu *et al*. 2023, Wangensteen *et al*. 2024).

Advancements in sensor technology have promoted the development of guided wave methods. Compared with the piezoelectric transducer, the magnetostrictive (MS) transducer is more frequently used for steel strands because of its noncontact nature (Kim and Kwon 2015). The MS transducer commonly consists of permanent magnets and a coil unit. Under the combination of a longitudinal static bias magnetic field and a dynamic alternating magnetic field, the longitudinal guided waves can be excited in the steel strand. Kwun and Teller (1994) manufactured a MS transducer and applied it for wire breakage detection. Lee and Kim (2002) further refined the technology by introducing different types of permanent magnets to control the generated wave modes. Laguerre *et al*. (2002) suggested replacing the permanent magnet with a solenoid coil and explored the effects of driving voltage on the excitation signal. The energy conversion efficiency of the MS transducer is relatively low. To address this problem, multi-layer sensing coil units were presented, and the amplitudes of the excitation and received signals increased markedly (Liu *et al*. 2010, Tse *et al*. 2011). However, the above studies focus more on the sensing unit and have not clarify the design criteria for the applied magnetic field, which has a significant influence on

*Corresponding author, Ph.D., Associate Professor,
E-mail: zhangru@hzcu.edu.cn
[a] Post Doctor, E-mail: xdsui@zju.edu.cn
[b] Professor, E-mail: ceyfduan@zju.edu.cn
[c] Professor, E-mail: luoyz@zju.edu.cn
[d] Professor, E-mail: ycb@zju.edu.cn

ISSN: 1738-1584 (Print), 1738-1991 (Online)

the amplitude of the generated signal. The noncontact nature of the MS transducer enables it to move freely along the steel strand, facilitating long sensing range. To the author's knowledge, the roving MS transducer system for wire breakage detection has not been reported. Additionally, the effect of lift-off distance between the MS transducer and the steel strand on the energy conversion efficiency for a roving detection system should be considered.

The potential of guided waves to detect local damages in steel strands has been proved by many studies. The propagated guided waves in the steel strand will be reflected when they encounter damage, allowing the damage conditions to be estimated by the damage-reflected and transmitted wave packets. Zhang *et al*. (2018) carried out the experiments on a 37-wire cable and successfully located wire breakages by analyzing the time of flight of the damage-reflected wave packets. Tang *et al*. (2021) proposed to evaluate the local damage severities of multiple wire breakages using the wave energy transmission coefficients at the damage locations. In addition to the time domain signal-based damage identification methods, Baltazar *et al*. (2010) proposed to detect the cable damages by analyzing the mode components of the received signals, noting that flexural modes were present when damage occurred. Duan *et al*. (2023) presented a method of transforming the received signals into topological patterns based on the persistent homology theory. Compared with other methods, such as the Fourier transformation amplitude spectrum-based method (Majhi *et al*. 2019) and the peak-to-peak ratio-based method (Raisutis *et al*. 2014), the topological feature-based method showed better performance. Zhou *et al*. (2023) introduced a cross-sparse representation-based wave packet separation method to reduce the interference signals and increase the damage detection accuracy. However, most of the proposed damage condition assessment methods require reference signals from the intact cases, which may not be available for the in-service steel strands. Farhidzadeh and Salamone (2015) developed a reference-free corrosion diagnosis method by measuring changes in wave velocity and wave mode components, but the damage severity cannot be well estimated. Therefore, it is essential to develop a practically reference-free method that boasts high accuracy in assessing damage conditions.

For damage detection in multi-wire steel strands, the wave energy transfer property between adjacent wires was investigated by many researchers (Haag *et al*. 2009, Schaal *et al*. 2016). The contact conditions were simulated by friction, viscous damper, and spring. Chen *et al*. (2022) investigated the attenuation characteristics of the guided wave propagating in the cable, considering the material damping, coupling conditions between wires, and heat energy. It has been found that the wave energy decays rapidly with increasing excitation frequency. The energy propagation attenuation was also large for a long sensing range. Thus, the wave packet reflected from damages occurred far from the sensor may not be detected by a fixed sensor detection system, resulting in a low damage detection accuracy.

This study proposes using a roving detector comprising a pair of MS transducers arranged in a pitch-catch type. The detector will move along the steel strand to obtain the received signals at different locations, thereby avoiding the energy attenuation problem. To reduce the dependence on reference signals, an outlier analysis was conducted on the wave energy of the received signal for damage localization and local damage severity estimation. In this paper, the dispersion analysis for multi-wire steel strands is introduced in Section 2. The working principle and design criterion of the MS transducer is presented in Section 3. An outlier analysis-based wire breakage detection method using a roving guided wave system with a pair of MS transducers is introduced in Section 4. Finite element (FE) simulations for wire breakage detection are carried out to validate the proposed method in Section 5. Experimental validations are also executed in Section 6. Finally, brief conclusions are provided in Section 7.

2. Dispersion analysis of multi-wire steel strands

This research was carried out on a seven-wire steel strand, comprising six helical wires encircling a straight wire. The primary geometrical and material properties of the strand are detailed in Table 1. The dispersion properties of the steel strand were studied at first to choose a proper wave mode and excitation frequency. A helical coordinate-based semi-analytical finite element (SAFE) method (Treyssède 2008) is employed in this study to analyze the dispersion properties of the steel strand. The displacement of the guided waves, denoted as $\mathbf{u}(x, y, h, t)$, was represented as follows

$$\mathbf{u}(x,y,h,t)=\begin{Bmatrix}u_x(x,y,h,t)\\u_y(x,y,h,t)\\u_z(x,y,h,t)\end{Bmatrix}=\begin{Bmatrix}u_x(x,y)\\u_y(x,y)\\u_h(x,y)\end{Bmatrix}e^{i(kh-\omega t)} \quad (1)$$

where, k is the wave number; ω is the angular frequency; h is the centerline of the helical wires. The wave propagated along the h-axis was assumed to be a harmonic exponential solution of the form $e^{i(kh-\omega t)}$. The cross-sectional area of the strand was meshed by 1290 nodes and 2266 triangular elements, as shown in Fig. 1(a). By solving the equation of motion in Eq. (2), the phase velocity and group velocity dispersive curves were obtained as in Fig. 1(b).

$$\int_\Omega \delta\boldsymbol{\varepsilon}^{\mathrm{T}}\boldsymbol{\sigma}\sqrt{g}dxdydh-\omega^2\int_\Omega \rho\delta\mathbf{u}^{\mathrm{T}}\mathbf{u}\sqrt{g}dxdydh=0 \quad (2)$$

where, $\boldsymbol{\sigma}$ and $\boldsymbol{\varepsilon}$ are the stress and strain vector; ρ is the density; g denotes the process variable, which is defined by the expression $g=(1+\kappa x)^2$; κ represents the curvature of the helical wire, calculated as $\kappa=4\pi^2R/l^2$, where R and l correspond to the radius and the curvilinear

Table 1 Geometrical and material properties of the steel strand with helical wires

Outer diameter (mm)	Diameter of wire (mm)	Peripheral pitch (mm)	Young's modulus (GPa)	Density (kg/m^3)	Poisson ratio
15.2	5.1	260	210	7850	0.28

(a) FE meshes of the cross section (b) Group velocity dispersion curve

Fig. 1 Dispersion analysis results of the seven-wire steel strand

length over a single pitch, respectively. Ω is the element volume.

As the excitation frequency exceeds 100 kHz, there is a significant increase in the number of wave modes, which can pose challenges for the identification of wave packets. Thus, the longitudinal L(0, 1) mode with an excitation frequency of 80 kHz was selected as the excitation signal. The group wave velocity of the L(0, 1) mode at 80 kHz was obtained as 4850 m/s, and the corresponding wavelength is 60.6 mm.

3. Design of the MS transducer

3.1 Working principle of the MS transducer

The magnetic domains within ferromagnetic materials will rotate under the influence of an external magnetic field, thereby generating MS strain. Conversely, micro-strain in ferromagnetic materials can also cause changes in the magnetic field. The relationship between the external applied magnetic field (H) and MS strain in a typical ferromagnetic material is shown in Fig. 2(a). To actuate varying guided waves, a dynamic excitation magnetic field is required. However, when the magnetic field fluctuates around point O, due to the MS strain on the steel strand always being positive, the excited guided wave signal will exhibit a double frequency phenomenon, as shown in Fig. 2(b). Therefore, a bias static magnetic field is needed to lift the initial magnetic field to point A, so that the relationship between H and MS strain may become close to linear. To enhance the energy of the excited guided waves, H_A should be positioned at the point of the maximum slope of the curve, which also corresponds to the point with the maximum permeability of the ferromagnetic material.

To generate the longitudinal guided waves, both the bias and the dynamic magnetic fields should be parallel to the axial direction of the steel strand. In this study, the bias magnetic field was provided by three sets of magnetizers, each set consisting of two permanent magnets and a yoke, thereby forming a closed magnetic field within the steel strand, as shown in Fig. 3. The dynamic magnetic field was generated by a solenoid coil.

3.2 Multi-physics analysis for magnetic induction

Multi-physics simulations were carried out on the MS transducer using a commercial software Maxwell. The purpose of the simulation analysis is to determine the size of the permanent magnets to ensure that the bias magnetic field is uniformly distributed across the cross-section of the steel strand, with the magnetic induction intensity close to the point of the maximum permeability (0.8 T). The NdFeB N35 permanent magnets were used with the geometrical and material properties listed in Table 2. Three sets of magnetizers were installed at equal angular intervals (120°) around the circumference of the steel strand as in Fig. 4(a). The FE meshes of the MS transducer was shown in Fig. 4(b). Finer meshes were introduced to the contact area between the steel strand and the permanent magnets for more accurate analysis.

The distribution of the magnetic induction intensity along the MS transducer was shown in Fig. 5(a). Figs. 5(b)-(d) illustrate the magnetic induction intensity on the cross-section of the steel strand at three distinct locations. Sections I and III are positioned close to the permanent magnets, while Section II is in the middle of the transducer (as well the location of the sensing coil). It can be observed

(a) Typical MS strain curve of a ferromagnetic material (b) The induced MS strain

Fig. 2 Relationship between the external applied magnetic field and the MS strain

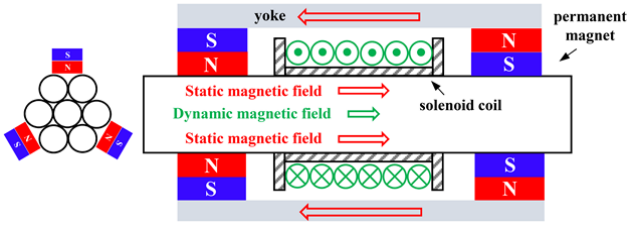

Fig. 3 Magnetic field distribution of the MS transducer for generating longitudinal guided waves

Table 2 Geometrical and material properties of the permanent magnet (yoke length = 70 mm)

Size (mm)	15 × 6 × 4	Density (g/cm^3)	7.45
Remanence (T)	1.17	Recoil permeability	1.05
Coercive force (kA/m)	867	Maximum magnetic energy product (kJ/m^3)	263

(a) Layout of the MS transducer

(b) FE meshes for multi-physics analysis

Fig. 4 FE model of the MS transducer

that the distribution of magnetic induction intensity at Section II is highly uniform under the current configuration, with magnitudes around 0.8 T. The length of the coil unit was designed as 30 mm, which is half of the wavelength (60.6 mm) of the excitation signal with 80 kHz.

4. Wire breakage condition assessment using a roving detector and outlier analysis

A pair of MS transducers were arranged in a pitch-catch type with a distance of d, which was used as a damage detector as shown in Fig. 6(a). The detector was designed to move freely along the steel strand to obtain the received signals at various locations. The wave energy (E) for the intact case at the receiver can be expressed as

$$E = E_0 e^{-\beta d} \tag{3}$$

where, E_0 is the energy of the excitation signal; β is the wave energy attenuation coefficient. E_0 is considered as constant, but the exact energy value may be very difficult to measure due to the uncertainty related to environment. β is related to the material damping, coupling conditions between wires, and the excitation frequency. β is assumed to be constant along the steel strand with a uniform cross section. Thus, in the absence of damage, the received wave energy at different locations of the detector along the steel strand will not change. Fig. 6(b) shows typical received signals under the intact and a damage case. The wave energy is defined as follows

$$E = \frac{1}{(t_2 - t_1)} \int_{t_1}^{t_2} y^2(t) dt \tag{4}$$

where, $y(t)$ is the received signal, which is filtered in a range of 60-100 kHz and then normalized by the maximum amplitude of the direct arrival wave packet for the intact case; t_1 is the time instant at which the signal arrives at the receiver. The interval between t_1 and t_2 corresponds to the time duration of the excitation signal. t_1 can be calculated by the distance between the transducers (d) and the measured wave velocity.

The position of the detector is denoted by r, which is equivalent to the distance between the receiver and the left end of the steel strand. As the detector moves close to the damage location, two distinct wave packets may be observed in the received signal, as shown in Fig. 7. The first wave packet corresponds to the direct arrival signal, whereas the second is the reflected wave from the damage. The damage-reflected wave packet arrives at the receiver at the time instant t_3. As the detector moves further, those two wave packets will overlap, resulting in a change in the received wave energy. Once the receiver has passed through the damage location while the damage still locates within the detector as in Fig. 6(a), the received wave energy of the transmitted wave will be stabilized to a reduced value representing the transmitted wave energy (E^{trans}) through the damage. The modified expression for the transmitted wave energy can be obtained as

$$E^{trans} = E_0 e^{-\beta d} \alpha \tag{5}$$

where, α is the wave energy transmission coefficient, which is related to the area remaining ratio at the damage location. The variation in the transmitted wave energy as the detector moves at different locations can be illustrated in Fig. 6(c), which facilitates the determination of the damage location and the local damage severity.

Influenced by the measurement noise, environmental factors, and equipment variability, the value of E^{trans} may exhibit fluctuations across different locations even in the intact cases. So, an outlier analysis was carried out to determine the threshold value E_{th} for damage detection. If

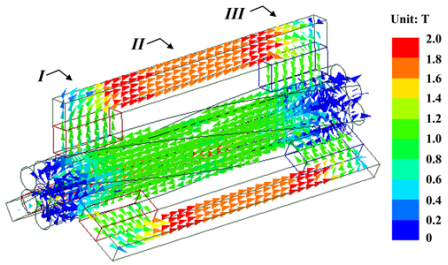

(a) Distribution of the magnetic induction intensity along the transducer and the steel strand

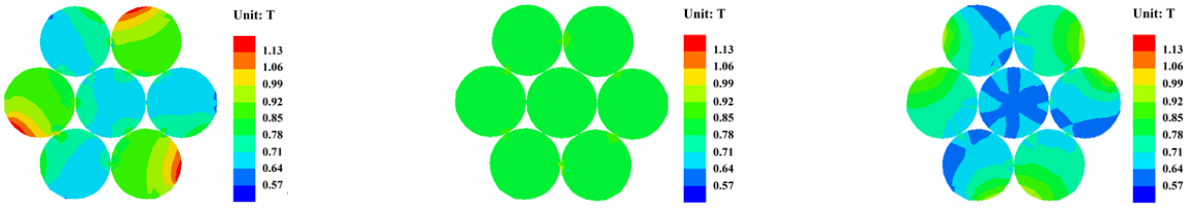

(b) Section I (c) Section II (d) Section III

Fig. 5 FE simulation results of the magnetic induction intensity on the transducer and the steel strand

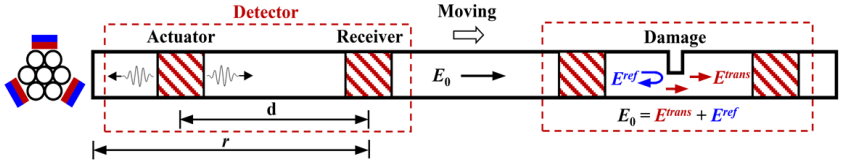

(a) Configuration of the damage detector

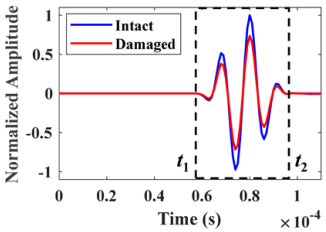

(b) Received signals under the intact and damaged cases

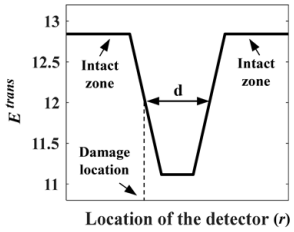

(c) Changes of the transmitted wave energy at different locations

Fig. 6 Damage detection using the roving MS transducers

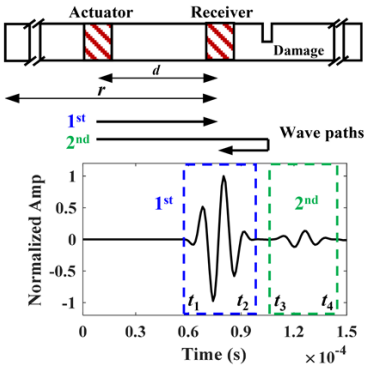

Fig. 7 Received signal with the detector close to the damage

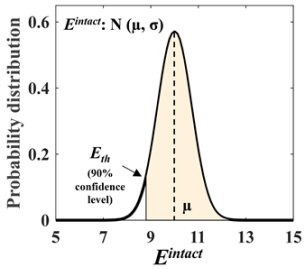

Fig. 8 Estimation of the threshold Eth by probability distribution analysis

the measured E^{trans} is smaller than E_{th}, it is inferred that damage is present between the actuator and the receiver. The outlier analysis is conducted by two steps. First, numerous received signals are gathered from different locations under the intact case. Noted that these intact signals can be obtained along a steel strand with the same geometrical and material properties to the tested one. These collected signals are normalized by the maximum value of the received signal. In the second step, the wave energy E_i^{intact} for the *i*th received signal will be calculated by Eq. (4). The Gaussian probability distribution of E^{intact} is estimated from many intact cases as N(μ, σ), where μ and σ

are the mean and standard deviation. E_{th} is derived with a 90% confidence level from this distribution as shown in Fig. 8. Finally, the wave energy transmission coefficient (α) is determined for local damage severity estimation based on the transmitted wave energy in the damaged case ($E^{trans,dam}$) and the mean value (μ) of the intact case as follows

$$\alpha = \sqrt{E^{trans,dam}/\mu} \tag{6}$$

5. Numerical simulation study

5.1 FE model

A FE model of a seven-wire steel strand in a helical mode was constructed for the guided wave analysis using ABAQUS to assess the feasibility of the proposed wire breakage detection method. The length of the steel strand model was taken as 1040 mm, with the geometrical and material properties consistent with those listed in Table 1. The actuator and receiver of the damage detector were separated by a distance (d) of 300 mm, and the detector moved to the next case by an interval of 100 mm, as illustrated in Fig. 9. Wire breakages with a width of 1.5 mm were set on the outer layer at a distance of 520 mm from the right end of the strand. Four damage cases were simulated at the same location to estimate the damage severity with the damage scenarios listed in Table 3. The excitation signal was taken as a 3-cycled sinusoidal tone burst with the central frequency of 80 kHz as shown in Fig. 10. The mesh size was selected as 1.5 mm in the axis direction, ensuring that at least 20 nodes exist within the wavelength (60.6 mm). The FE model consists of 92411 nodes and 60973 linear solid hexahedral eight-node elements. The excitation signal was simulated by applying the nodal displacements on the cross section of the steel strand. An explicit dynamic analysis was carried out for the wave propagation process. The integration time step was automatically selected, and the sampling frequency was 1 MHz. The wave energy attenuation was not considered for the roving detector with a short distance between two transducers ($\beta = 1$).

5.2 FE simulation results

The received signals at various detection locations (r) under the intact case are shown in Fig. 11. The direct arrival wave packets were used for the wire breakage condition assessment. The wave velocity was calculated from the time of flights of the guided wave signals as 5084 m/s with a difference of 4% from the SAFE analysis result. The received wave energies (E^{intact}) were around 2.11 (dimensionless quantity as defined in Eq. (4)) at all the receiver locations. In simulation, this value will not change. Thus, both of E_{th} and μ were taken as 2.11.

Table 3 Number of broken wires for 4 damage cases

Damage cases	1	2	3	4
Number of the broken wires	0.5	1	1.5	2

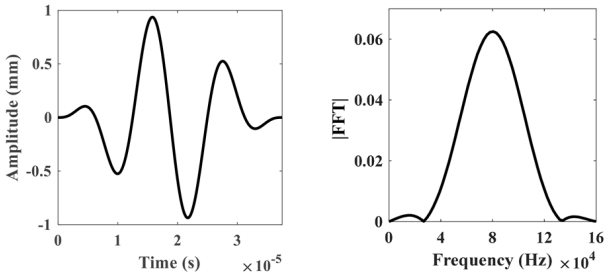

(a) Time history (b) FFT

Fig. 10 Tone burst excitation signal with 3 cycles

The direct arrival wave packets in four damage cases are shown in Fig. 12, when the detector position (r) is set to 700 mm. It can be observed that the amplitude decreased gradually by increasing the damage severity. The transmitted wave energies computed at various detector locations (r) for the four damage cases are shown in Fig. 13. When r equals 600, 700, and 800 mm, the wave transmitted wave energy becomes smaller than E_{th}, which indicates that wire breakage occurred between the actuator and the receiver. The $E^{trans,dam}$ was determined by the average value at the above three locations. The energy transmission coefficient (α) was then computed using Equation (6) for each damage case. The energy transmission coefficients are generally closely related to the area remaining ratios at the damage location, though they are not theoretically equal, particular for non-circular cross sections and non-axisymmetric damages. The maximum difference between the two quantities is found to be 3.3% as listed in Table 4, indicating excellent performance for the wire breakage severity estimation.

However, the transmitted wave energy is also smaller than the E_{th} when r equals 500 mm belonging to the intact region. The reason is that the damage at 520 mm is quite close to the receiver as in Fig. 7, making the transmitted

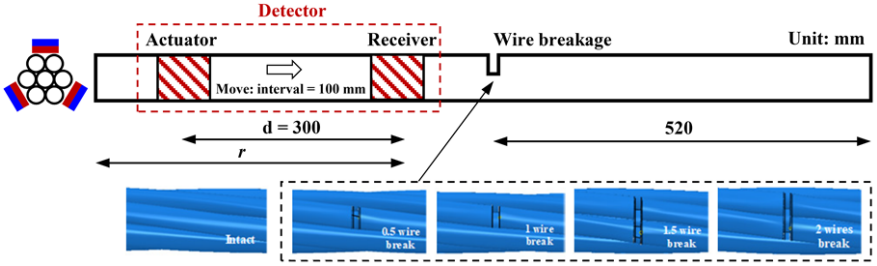

Fig. 9 Layout of a steel strand and wire breakage for 4 damage cases: width of the cut 1.5 mm

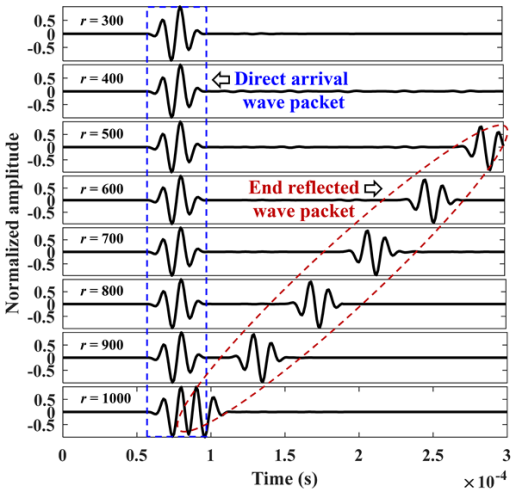

Fig. 11 Received signals at various locations under the intact case (FE simulation)

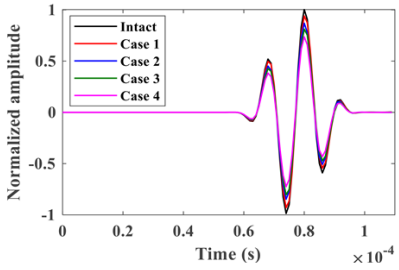

Fig. 12 Received signals under different damage cases (r = 700 mm)

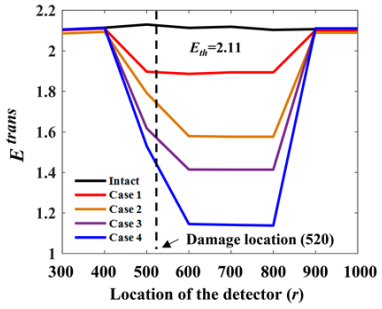

Fig. 13 Changes of E^{trans} under different damage cases

Table 4 Wire breakage severity estimation results: simulation analysis

Damage cases	α	Area remaining ratios	Differences
1	0.947	0.929	1.8%
2	0.864	0.857	0.7%
3	0.819	0.786	3.3%
4	0.736	0.714	2.2%

wave interfered by the damage-reflected wave. The received signals at three locations (r = 400, 500, and 600 mm) under Damage Case 2 are shown in Fig. 14. Upon

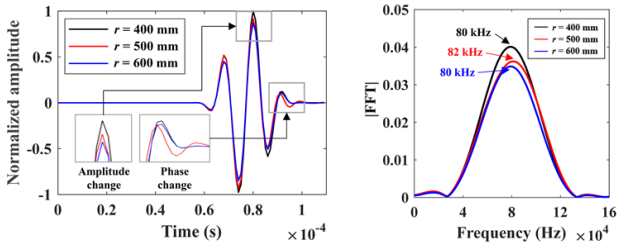

(a) Time domain (b) Frequency domain

Fig. 14 Received signals at three detection locations (r = 400, 500, and 600 mm) under Damage Case 2

increasing r from 400 mm to 500 mm, there is a notable change in both the amplitude and phase of the directly arriving wave packet. Additionally, the central frequency of the received signal shifted from 80 kHz to 82 kHz. When r is further increased to 600 mm, a comparison with the signal at r = 400 mm reveals a change in amplitude with no corresponding phase alteration. The above phenomenon may be used for wire breakage localization.

5.3 Comparison with a fixed damage detection system

The performance of the proposed roving detector was compared with that of a fixed damage detection system used in our previous study (Tang *et al*. 2021), through FE simulations conducted on a longer steel strand. The length of the steel strand is 10.4 m. The wire cross-section properties and breakage conditions are taken as same to those in Table 3. The wire breakage occurs at 2.6 m away from the right end as shown in Fig. 15. The excitation signal was applied at the left end of the steel strand, and the signal was captured by a fixed receiver positioned 0.6 m from the same end. The current FE model cannot properly simulate the coupling conditions between wires, thus material damping was added to simulate the wave energy attenuation phenomenon. The wave energy attenuation coefficient β obtained in simulation is 0.393 (per m), which is slightly smaller than the value in the experiment shown in Section 6. Fig. 16 shows the received signal with one wire break, delineating five wave packets. The first wave packet corresponds to the direct arrival, whereas the second and third are those reflected from the damage location. The fourth and fifth are those reflected from the right end of the strand. The amplitudes of the damage-reflected and end reflected wave packets are much smaller than the direct arrival wave packet. Considering the larger wave energy attenuation coefficient and measurement noise in real application, the damage-reflected wave packets may be even harder to be recognized. Wavelet transform analysis was performed on the received signals, and the wave energy transmission ratio (α_{fixed}) was calculated for four damage cases. This computation was executed by including the wave energy attenuation coefficient β in Equation (3), and the results are listed in Table 5. The α_{fixed} values were also compared with the area remaining ratios, with the maximum difference of 16.1%, indicating poorer performance than the proposed roving damage detection

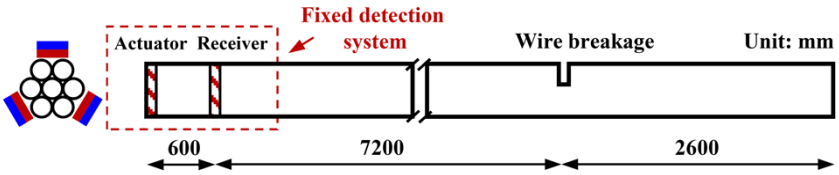

Fig. 15 Layout for a fixed damage detection system on a long steel strand of 10.4 m

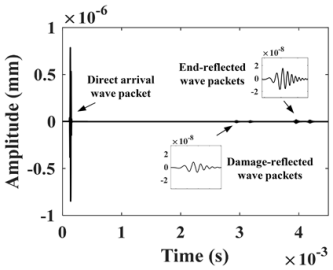

Fig. 16 Received signal with one wire break by the fixed damage detection system

Table 5 Wire breakage severity estimation using a fixed damage detection system

Damage cases	α_{fixed}	Area remaining ratios	Differences
1	0.997	0.929	6.8%
2	0.967	0.857	11.0%
3	0.947	0.786	16.1%
4	0.867	0.714	15.3%

system. Furthermore, the fixed detection system may overlook small damage-reflected wave packets due to the large wave energy attenuation along the long propagation path, potentially leading to the neglect of such signals in practical applications.

5.4 Case of a larger cable with 19 wires

FE simulations were also carried out on a cable with 19 wires to detect the wire breakage conditions. The cross section of the cable is shown in Fig. 17. The diameter of single wire is 5 mm, and the material properties are the same as those in Table 1. The wires were arranged in parallel, which is commonly used in engineering applications. The length of the cable was also 1040 mm, and the wire breakage was set on the outer layer. The distance between the actuator and the receiver was 300 mm, and the moving interval was 100 mm. The modeling method for the cable was the same as that in Section 5.1, but the central frequency of the excitation signal was changed to 30 kHz due to severe dispersion in the high frequency region (Zhang et al. 2018). Three damage conditions were considered, with the number of broken wires being 2, 4, and 6, and the wire breakage severity estimation results were listed in Table 6. The maximum difference between the energy transmission coefficient (α) and the area remaining ratio at the damage location was 0.2%, indicating excellent performance of the proposed

Fig. 17 Cross section of a cable with 19 wires

Table 6 Wire breakage severity estimation results for a cable with 19 wires: simulation analysis

Number of broken wires	α	Area remaining ratios	Differences
2	0.894	0.895	0.1%
4	0.787	0.789	0.2%
6	0.683	0.684	0.1%

The dispersion properties of cables with large diameters are more complex. The frequency range with weaker dispersion gets shortened as discussed by Zhang *et al.* (2018), which means that the appropriate excitation frequency range is limited. Additionally, proper configurations of the MS transducer shall be designed to provide a uniform static magnetic field for the cables with large diameters.

6. Experimental study

6.1 Experimental setup

Experimental tests were also conducted on a seven-wire steel strand, mirroring the geometrical and material properties of the FE model to substantiate the proposed damage detection method. The layout of the test specimen and detector is shown in Fig. 18 with a total length of 2700 mm. The distance between the actuator and receiver was maintained at 600 mm. In order to avoid the overlapping of the direct arrival and left end-reflected wave packets, the initial location of the actuator was taken as 250 mm away from the left end of the steel strand. The moving interval of the detector was set as 200 mm during the tests. Artificial wire breakage with a width of 1.5 mm was imposed in the middle of the test specimen using a cutting machine. The same four damage cases as in Table 3 were considered. The excitation signal was generated and amplified by the testing equipment developed by Hangzhou Zheda Jingyi Electromechanical Technology Co., LTD. The received signal was amplified and displayed using the same equipment. The sampling frequency was 1 MHz. A personal

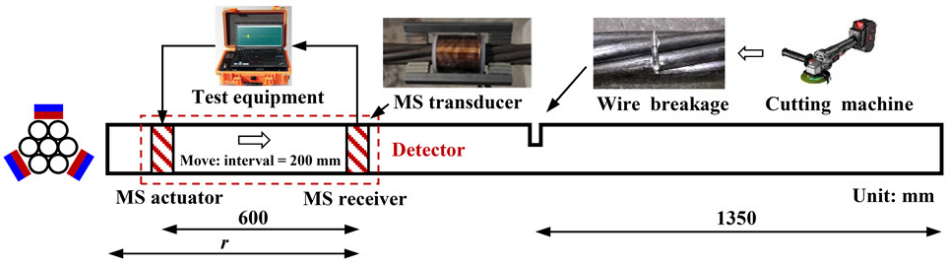

Fig. 18 Layout of the test specimen and roving detector: Length = 2.7 m

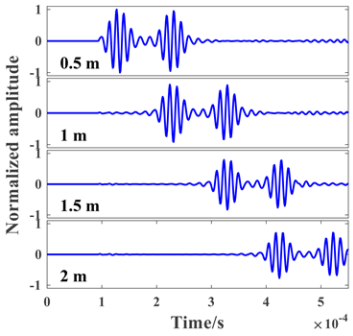

(a) Received signals at four receiver locations

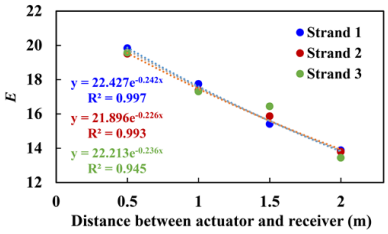

(b) Determination of wave energy attenuation coefficients

Fig. 19 Wave energy attenuation tests for three steel strands

laptop was used for setting the test parameters and data collection.

6.2 Determination of the E_{th} from the intact cases

As mentioned in Section 4, the received signals are sensitive to ambient factors. Thus, a large population of signals was collected from three steel strands of identical dimensions under the intact case to determine the E_{th} and μ. First, the wave energy attenuation coefficients β for three steel strands were obtained to figure out their differences. In this test, the actuator was positioned 250 mm from the left end, while the receiver moved at four different locations: 0.5 m, 1 m, 1.5 m, and 2 m away from the actuator. Fig. 19(a) displays the received signals at these four locations for one of the steel strands. The first wave packet is the direct arrival signal, while the second wave packet is the reflected one from the left end. The wave velocity was obtained as 4856 m/s, which is very close to the SAFE analysis result of 4850 m/s. Fig. 19(b) shows the wave energies derived from all measured signals computed by Eq. (4), which were fitted with an exponential form. The wave energy attenuation coefficients (β) were obtained as 0.451, 0.433, and 0.444 (per m) for the three steel strands, with coefficient of determination R^2 values of 0.998, 1, and 0.978, respectively. Therefore, the wave propagation properties of the three test specimens were similar.

Then, the detector with an actuator and a receiver was moved at 36 different locations for each steel strand, resulting in a total of 108 measured groups of signals. For each signal, the wave energy E^{intact} was calculated, and the collective probability distribution was depicted in Fig. 20. The Gaussian probability density function for E^{intact} was

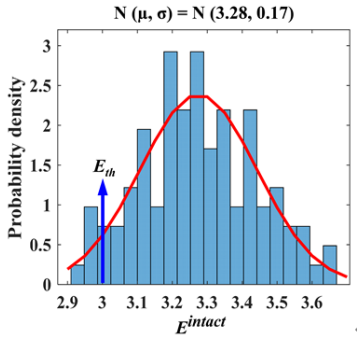

Fig. 20 Wave energy distribution for the intact cases and determination of the threshold value

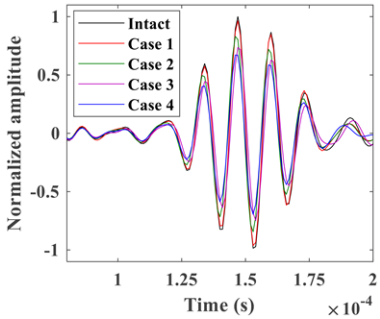

Fig. 21 Received signals under four damage cases (r = 1650 mm): experiment

characterized as N(3.28, 0.17). Utilizing a 90% confidence level, the threshold value E_{th} was established for damage detection as 3.

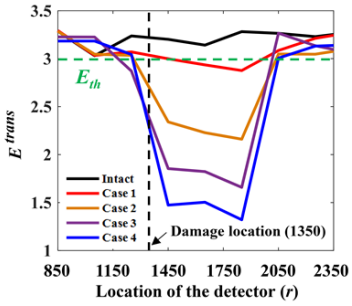

Fig. 22 Changes of the transmitted wave energy under four damage cases

Table 7 Wire breakage severity estimation results: experiments

Damage cases	α	Area remaining ratios	Differences
1	0.947	0.929	1.8%
2	0.827	0.857	3.0%
3	0.736	0.786	5.0%

6.3 Wire breakage detection results

The number of broken wires was gradually increased from 0.5 to 2 at the same location (1.35 m from the left end) to assess the detection capabilities of the proposed method. The received signals corresponding to different damage severities, with a detector position r of 1650 mm, were shown in Fig. 21. As anticipated, the amplitude of the direct arrival wave packet decreased with increasing damage severity. Fig. 22 illustrates the wave energies at various detector locations (r) under four damage cases. Similarly, the average wave energy measured at three locations (r = 1450, 1650, and 1850 mm) was used for the damage severity estimation with the results summarized in Table 7. The estimated wave energy transmission coefficients (α) agree very well to the area remaining ratios at the wire breakage locations with a maximum difference of 5.4%. The estimated α is excellent even for Damage Case 1 with a half wire broken, indicating that the proposed wave energy method is better than the maximum amplitude change-based method (Zhang *et al*. 2018).

6.4 Influence of the lift-off distance

In practical applications, steel strands or cables with larger diameters are often encased in a polyethylene sheath, which precludes direct attachment of the MS transducer to the steel strand. Moreover, the large magnetic forces induced by powerful magnets make it difficult to maneuver the MS transducer along the steel strand. Conversely, weaker magnets may fail to provide a sufficient static magnetic field within the steel strand. So, a lift-off distance is present between the MS transducer and the steel strand. A series of experiments were carried out to examine the influence of the lift-off distance on the damage detection accuracy. Fig. 23(a) displays the received signals under the intact case with a lift-off distance of 2 mm and 3 mm. With the same driving voltage, the maximum amplitude of the received signals decreased from 0.075 V to 0.061 V and further to 0.047 V as the lift-off distance was increased to 2 mm and 3 mm, respectively. In real applications, the effect of the lift-off distance shall be considered in the design process of the MS transducer to determine proper size of the permanent magnets. Furthermore, the excitation power may also be enlarged to reduce signal attenuation. The received signals at the damaged cases were normalized against the signal from the intact case before calculating the transmitted wave energies. Fig. 23(b) shows the wave energies for different lift-off distances under Damage Case 2. The wave energy transmission coefficients were measured at 0.834 and 0.829 for the cases with lift-off distances of 2 mm and 3 mm, respectively. Those values are found to be very close to the area remaining ratio (0.857) for one wire break.

6.5 Discussion

For wire breakage detection of long steel strands or cables, wave energy attenuation can be substantial. Traditional methods that rely on damage-reflected signals may prove ineffective due to the diminished amplitude of the reflected wave packets. The proposed method mitigates the impact of wave energy attenuation and can be achieved with the assistance of a cable climbing robot as shown in Fig. 24 (Xu *et al*. 2021). Experiments are going to be conducted on long cables with a cable climbing robot in the next stage. Currently, cable climbing robots are usually equipped with visual sensing units to detect surface damage on the cable (Ho *et al*. 2013). By integrating the MS

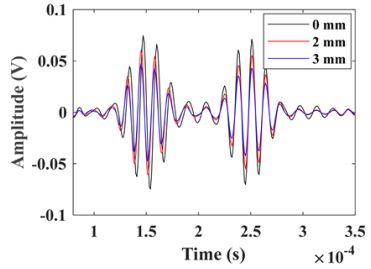

(a) Received signals with different lift-off distances under the intact case

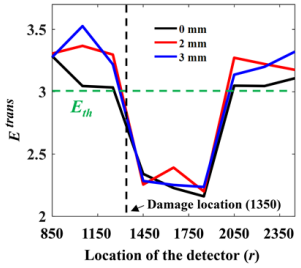

(b) Wave energies with different lift-off distances under Damage Case 2

Fig. 23 Influence of the lift-off distance on the damage detection accuracy

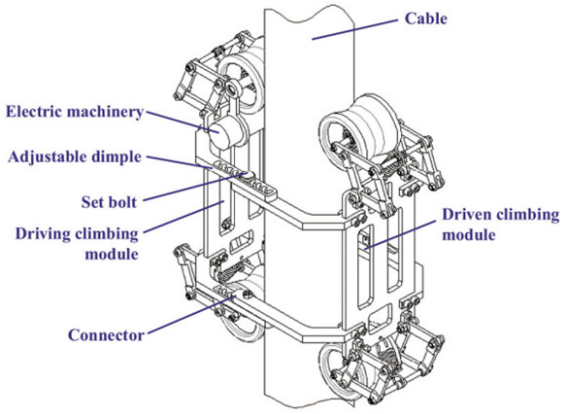

Fig. 24 Lightweight cable climbing robot (Xu *et al*. 2021)

transducer, the assessment of internal damages becomes feasible. The half-cylindrical sensing coil may be practical and useful for mounting and dismounting on existing cables, which will be studied in the future. Additionally, the proposed method is applicable to the detection of damages in moving cables, such as those used in elevators. In such cases, the proposed damage detector can be stationed at a fixed position. Given that the guided wave velocity significantly exceeds the operational speed of elevators, real-time cable damage detection is achievable.

To determine the E_{th} for damage localization and damage severity estimation, the received signals at various locations on the steel strand under the intact cases are needed. Intact signals may be obtained from a steel strand with identical properties or the intact portion of the cable under test as in Section 6.2. This roving detector minimizes the necessity for reference signals under the intact conditions, making it practically reference-free.

However, the effects of environmental factors, such as temperature and humidity, and variations in external forces on the received signals warrant further investigation. Future research will also explore the impact of various wave modes and central frequencies of the excitation signal to enhance the sensitivity of wire breakage detection, particularly in the early stages of damage.

7. Conclusions

In this study, an outlier analysis method has been presented for wire breakage detection of a seven-wire steel strand using a roving MS transducer system based on longitudinal guided waves. The problem of significant wave energy attenuation over long propagation distances, which can impair the damage estimation accuracy, has been addressed by the proposed method. The dispersion properties of the multi-wire steel strand were analyzed using the SAFE method. A damage detector, comprising two MS transducers, was utilized to acquire guided wave signals and transmitted wave energies at various locations along the steel strand. Then, the outlier analysis was performed by taking the transmitted wave energy as a damage-sensitive feature. The threshold value for damage judgment was determined from the probability distribution of the transmitted wave energies under the intact cases. From numerical and experimental studies on the steel strand with varying wire breakage severities, the following conclusions can be drawn:

(1) Wire breakages were effectively detected using the proposed MS transducer-based roving damage detector and the transmitted wave energy-based outlier analysis. Variations in the transmitted wave energy were instrumental in localizing the damage.
(2) Damage severities were accurately assessed using the wave energy transmission coefficients derived from the roving detector, which demonstrated strong correlations with the area remaining ratios at the damage location. The maximum differences observed were 3.3% for numerical simulations and 5.4% for experimental tests, respectively.
(3) The proposed roving detector-based wire breakage detection method was practically reference-free, and the performance for damage severity estimation was much better than the fixed detection system, particularly for long steel strands.
(4) An increase in lift-off distance between the MS transducer and the steel strand diminishes the amplitudes of the received signals. Nonetheless, the wire breakage condition can still be reliably evaluated by the proposed method.

Acknowledgments

This work was supported by the Zhejiang Provincial Natural Science Foundation of China (Grant No. LGG21E080004), Scientific Research Fund of Zhejiang Provincial Education Department (Grant No. Y202454348), and National Natural Science Foundation of China (Grant Nos. U24A20169, 51608478).

References

Abdullah, A.B.M., Rice, J.A. and Hamilton, H.R. (2015), "A strain-based wire breakage identification algorithm for unbonded PT tendons", *Smart Struct. Syst., Int. J.*, **16**(3), 415-433. https://doi.org/10.12989/sss.2015.16.3.415

Baltazar, A., Hernandez-Salazar, C.D. and Manzanares-Martinez, B. (2010), "Study of wave propagation in a multiwire cable to determine structural damage", *NDT & E Int.*, **43**(8), 726-732. https://doi.org/10.1016/j.ndteint.2010.08.007

Chen, X., Zhu, J.S. and Lin, Y.Z. (2022), "Attenuation characteristics of low frequency longitudinal guided waves generated by magnetostrictive transducers in bridge cables", *Mech. Syst. Signal Process.*, **164**, 108296. https://doi.org/10.1016/j.ymssp.2021.108296

Christen, R., Bergamini, A. and Motavalli, M. (2009), "Influence of steel wrapping on magneto-inductive testing of the main cables of suspension bridges", *NDT & E Int.*, **42**(1), 22-27. https://doi.org/10.1016/j.ndteint.2008.08.003

Duan, Y.F., Sui, X.D., Tang, Z.F. and Yun, C.B. (2022), "Bolt looseness detection and localization using time reversal signal and neural network techniques", *Smart Struct. Syst., Int. J.*, **30**(4), 397-410. https://doi.org/10.12989/sss.2022.30.4.397

Duan, S.Y., Wu, X.J., Zou, Y.Q. and Jiang, L.J. (2023), "Corrosion characterization of steel wires based on persistent homology theory for magnetostrictive guided wave testing signal", *Struct. Health Monitor. – Int. J.*, **22**(3), 2147-2165. https://doi.org/10.1177/14759217221119790

Dubuc, B., Ebrahimkhanlou, A. and Salamone, S. (2018), "Higher order longitudinal guided wave modes in axially stressed seven-wire strands", *Ultrasonics*, **84**, 382-391. https://doi.org/10.1016/j.ultras.2017.12.003

Farhidzadeh, A. and Salamone, S. (2015), "Reference-free corrosion damage diagnosis in steel strands using guided ultrasonic waves", *Ultrasonics*, **57**, 198-208. https://doi.org/10.1016/j.ultras.2014.11.011

Haag, T., Beadle, B.M., Sprenger, H. and Gaul, L. (2009), "Wave-based defect detection and interwire friction modeling for overhead transmission lines", *Arch. Appl. Mech.*, **79**(6-7), 517-528. https://doi.org/10.1007/s00419-008-0282-x

Ho, H.N., Kim, K.D., Park, Y.S. and Lee, J.J. (2013), "An efficient image-based damage detection for cable surface in cable-stayed bridges", *NDT & E Int.*, **58**, 18-23. https://doi.org/10.1016/j.ndteint.2013.04.006

Ibáñez, F., Baltazar, A. and Mijarez, R. (2015), "Detection of damage in multiwire cables based on wavelet entropy evolution", *Smart Mater. Struct.*, **24**(8), 085036. https://doi.org/10.1088/0964-1726/24/8/085036

Kharrat, M. and Gaillet, L. (2015), "Non-destructive evaluation of anchorage zones by ultrasonics techniques", *Ultrasonics*, **61**, 52-61. https://doi.org/10.1016/j.ultras.2015.03.007

Kim, Y.Y. and Kwon, Y.E. (2015), "Review of magnetostrictive patch transducers and applications in ultrasonic nondestructive testing of waveguides", *Ultrasonics*, **62**, 3-19. https://doi.org/10.1016/j.ultras.2015.05.015

Kwun, H. and Teller, C.M. (1994), "Detection of fractured wires in steel cables using magnetorestrictive sensors", *Mater. Eval.*, **52**(4), 503-507.

Laguerre, L., Aime, J.C. and Brissaud, M. (2002), "Magnetostrictive pulse-echo device for non-destructive evaluation of cylindrical steel materials using longitudinal guided waves", *Ultrasonics*, **39**(7), 503-514. https://doi.org/10.1016/s0041-624x(01)00088-9

Lee, H. and Kim, Y.Y. (2002), "Wave selection using a magnetomechanical sensor in a solid cylinder", *J. Acoust. Soc. Am.*, **112**(3), 953-960. https://doi.org/10.1121/1.1497623

Liu, Z.H., Zhao, J.C., Wu, B., Zhang, Y.N. and He, C.F. (2010), "Configuration optimization of magnetostrictive transducers for longitudinal guided wave inspection in seven-wire steel strands", *NDT & E Int.*, **43**(6), 484-492. https://doi.org/10.1016/j.ndteint.2010.05.003

Majhi, S., Mukherjee, A., George, N.V. and Uy, B. (2019), "Corrosion detection in steel bar: a time-frequency approach", *NDT & E Int.*, **107**, 102150. https://doi.org/ 10.1016/j.ndteint.2019.102150

Ng, C.T., Yeung, C.R., Yin, T.Y. and Chen, L.J. (2022), "Stress evaluation of tubular structures using torsional guided wave mixing", *Smart Struct. Syst., Int. J.*, **30**(6), 639-648. https://doi.org/10.12989/sss.2022.30.6.639

Nguyen, K.D. and Kim, J.T. (2012), "Smart PZT-interface for wireless impedance-based prestress-loss monitoring in tendon-anchorage connection", *Smart Struct. Syst., Int. J.*, **9**(6), 489-504. https://doi.org/10.12989/sss.2012.9.6.489

Raisutis, R., Kazys, R., Mazeika, L., Zkauskas, E., Samaitis, V. and Jankauskas, A. (2014), "Ultrasonic guided wave-based testing technique for inspection of multi-wire rope structures", *NDT & E Int.*, **62**, 40-49. https://doi.org/10.1016/j.ndteint.2013.11.005

Rizzo, P. and di Scalea, F.L. (2006), "Wavelet-based feature extraction for automatic defect classification in strands by ultrasonic structural monitoring", *Smart Struct. Syst., Int. J.*, **2**(3), 253-274. https://doi.org/10.12989/sss.2006.2.3.253

Rostami, J., Tse, P.W. and Yuan, M.D. (2020), "Detection of broken wires in elevator wire ropes with ultrasonic guided waves and tone-burst wavelet", *Struct. Health Monitor. – Int. J.*, **19**(2), 481-494. https://doi.org/10.1177/1475921719855915

Schaal, C., Bischoff, S. and Gaul, L. (2016), "Damage detection in multi-wire cables using guided ultrasonic waves", *Struct. Health Monitor. – Int. J.*, **15**(3), 279-288. https://doi.org/10.1177/1475921716642747

Setshedi, II, Loveday, P.W., Long, C.S. and Wilke, D.N. (2019), "Estimation of rail properties using semi-analytical finite element models and guided wave ultrasound measurements", *Ultrasonics*, **96**, 240-252. https://doi.org/10.1016/j.ultras.2018.12.015

Tang, Z.F., Sui, X.D., Duan, Y.F., Zhang, P.F. and Yun, C.B. (2021), "Guided wave-based cable damage detection using wave energy transmission and reflection", *Struct. Control Health Monitor.*, **28**(5), e2688. https://doi.org/10.1002/stc.2688

Treyssède, F. (2008), "Elastic waves in helical waveguides", *Wave Motion*, **45**(4), 457-470. https://doi.org/10.1016/j.wavemoti.2007.09.004

Tse, P.W., Liu, X.C., Liu, Z.H., Wu, B., He, C.F. and Wang, X.J. (2011), "An innovative design for using flexible printed coils for magnetostrictive-based longitudinal guided wave sensors in steel strand inspection", *Smart Mater. Struct.*, **20**(5), 055001. https://doi.org/10.1088/0964-1726/20/5/055001

Tu, J.Q., Xu, X., Yun, C.B. and Duan, Y.F. (2023), "Ultrasonic guided waves-based fatigue crack detection in a steel I-beam: an experimental study", *Smart Struct. Syst., Int. J.*, **31**(1), 13-27. https://doi.org/10.12989/sss.2023.31.1.013

Wangensteen, M., Johansen, T.F., Fatemi, A. and Viggen, E.M. (2024), "Pipe wall thickness estimation by frequency-wavenumber analysis of circumferential guided waves", *Mech. Syst. Signal Process.*, **215**, 111369. https://doi.org/10.1016/j.ymssp.2024.111369

Wu, J.Y., Lan, C.M., Xian, G.J. and Li, H. (2018), "Recognition of damage pattern and evolution in CFRP cable with a novel bonding anchorage by acoustic emission", *Smart Struct. Syst., Int. J.*, **21**(4), 421-433. https://doi.org/10.12989/sss.2018.21.4.421

Xu, F.Y., Dai, S.Y., Jiang, Q.S. and Wang, X.S. (2021), "Developing a climbing robot for repairing cables of cable-stayed bridges", *Automat. Constr.*, **129**, 103807. https://doi.org/ 10.1016/j.autcon.2021.103807

Zhang, P.F., Tang, Z.F., Duan, Y.F., Yun, C.B. and Lv, F.Z. (2018), "Ultrasonic guided wave approach incorporating SAFE for detecting wire breakage in bridge cable", *Smart Struct. Syst., Int. J.*, **22**(4), 481-493. https://doi.org/10.12989/sss.2018.22.4.481

Zhou, J.X., Lin, J.F., Hong, X.B. and Yang, D.M. (2023), "Cross-sparse representation based on dispersion dictionary for ultrasonic guided wave to messenger cable damage detection in cladding zone", *Struct. Health Monitor. – Int. J.*, **22**(5), 3141-3164. https://doi.org/10.1177/14759217221140971